The EUMETSAT Network of Satellite Application Facilities

OSI SAF
Ocean and Sea Ice

Algorithm Theoretical Basis Document for the OSI SAF Global Sea Ice Concentration Climate Data Record

OSI-450

Version 1.1

7 July 2016

Thomas Lavergne, Rasmus Tonboe, John Lavelle and Steinar Eastwood

This page is intentionally left blank.

Document Change Record

Version	Date	Change	Description	Responsible
1.0	23.06.2016		First version for review	John Lavelle
1.1	7.7.2016		Edited after PCR comments	John Lavelle

Table of Contents

1 Introduction....5
1.1 The EUMETSAT Ocean and Sea Ice SAF....5
1.2 Scope....5
1.3 Overview....5
1.4 Glossary....6
1.5 Applicable documents....7
2 Input Data....8
2.1 The SMMR data....8
2.2 The SSM/I data....8
2.3 The SSMIS data....9
2.4 The ERA-Interim data....10
3 Algorithms....11
3.1 Land spill-over correction of brightness temperatures....11
3.2 Level-2 algorithms....12
3.2.1 The SICCI2 hybrid algorithms....12
3.2.2 Dynamic SIC algorithms from triplet of Tbs....13
3.2.3 Atmospheric correction of Tb....16
3.2.3.1 The radiative transfer model function for open water and sea ice....16
3.2.3.2 Iterative double-difference scheme for atmospheric correction....17
3.2.4 Dynamical 0% and 100% SIC training samples....17
3.2.4.1 The closed-ice samples....17
3.2.4.2 The open water samples....18
3.2.4.3 Dynamic tuning: constantly updating the training samples....20
3.2.5 Weather Filter....20
3.2.6 Level-2 uncertainties....21
3.2.6.1 Algorithm and tie-point uncertainty....22
3.2.6.2 Uncertainty for the hybrid SICCI2LF algorithm....23
3.3 Level 3 algorithms....23
3.3.1 Gridding and daily averaging....24
3.3.2 Gridding and smearing uncertainty....24
3.3.3 Climatological maximum extent masking....25
3.3.4 Possible melting or high T2m flag....25
3.4 Level 4 algorithms....25
3.4.1 Gap filling by interpolation....25
3.4.1.1 Temporal interpolation....26
3.4.1.2 Spatial interpolation....26
3.4.2 Total uncertainty....26
4 Conclusions....28
5 References....29

1 Introduction

1.1 The EUMETSAT Ocean and Sea Ice SAF

The Satellite Application Facilities (SAFs) are dedicated centres of excellence for processing satellite data – hosted by a National Meteorological Service – which utilise specialist expertise from institutes based in Member States. EUMETSAT created Satellite Application Facilities (SAFs) to complement its Central Facilities capability in Darmstadt. The Ocean and Sea Ice Satellite Application Facility (OSI SAF) is one of eight EUMETSAT SAFs, which provide users with operational data and software products. More on SAFs can be read at www.eumetsat.int.

OSI SAF produces (on an operational basis) a range of air-sea interface products, namely: wind, sea ice characteristics, Sea Surface Temperatures (SST), Surface Solar Irradiance (SSI) and Downward Longwave Irradiance (DLI). The sea ice products include sea ice concentration, the sea ice emissivity at 50 GHz, sea ice edge, sea ice type and sea ice drift and sea ice surface temperature (from mid 2014).

The OSI SAF consortium is hosted by Météo-France. The sea ice processing is performed at the High Latitude processing facility (HL centre), operated jointly by the Norwegian and Danish Meteorological Institutes.

Note: The ownership and copyrights of the data set belong to EUMETSAT. The data is distributed freely, but EUMETSAT must be acknowledged when using the data. EUMETSAT's copyright credit must be shown by displaying the words "copyright (year) EUMETSAT" on each of the products used. We welcome anyone to use the data. The comments that we get from our users is an important input when defining development activities and updates, and user feedback to the OSI SAF project team is highly valued...

1.2 Scope

This document is targeted at OSI SAF product users and describes the scientific background, the source data and the processing steps used to create the (OSI-450) OSI SAF Global Sea Ice Concentration Climate Data Record.

1.3 Overview

OSI-450 is the second major version of the OSI SAF Global Sea Ice Concentration Climate Data Record. The first version was called OSI-409, and was initiated in 2006 through visiting scientist activities with the UK Met Office and NSIDC. OSI-409 was extended at several occasions, using operational SSMIS and ECMWF data after 2009, but keeping the algorithms and processing chains unchanged.

OSI-450 is a full reprocessing of sea ice concentration, with improved algorithms and an upgraded processing chain, covering the period 1979 to 2015. The sea ice concentration is computed from the SMMR (1979-1987), SSM/I (1987-2008), and SSMIS (2006-2015) instruments, as well as ECMWF ERA-Interim data. The basis principles that were the backbone of OSI-409 are also on board OSI-450 (e.g. atmospheric correction of brightness temperature with NWP re-analysis data,

dynamic tie-points, uncertainties, etc.) but they were all revisited through dedicated R&D in the OSISAF project and, notably, through the ESA CCI Sea Ice projects.

Figure 1: The ESA Climate Change Initiative Sea Ice project contributed to OSI-450 through a number of algorithm developments.

From 2013 to 2018, the two ESA CCI Sea Ice projects conducted a series of thorough algorithms intercomparison exercises (Ivanova et al. 2015). They concluded that the methods and algorithms implemented in OSI-409 were the best available. In addition, they contributed to a number of algorithm developments and improvements that directly transfer into the OSI-450 algorithm baseline. In particular, OSI-450 uses the SICCI2LF algorithm, that was developed during the ESA CCI Sea Ice projects (Section 3.2.2). In exchange for algorithm improvements, the OSISAF offered re-use of its processing software for production of a complementary CDR by SICCI, based on the AMSR-E and AMSR2 instruments (2002-2011 and 2012-2015). The SICCI dataset is planned for Q4 2016. Potential users of the SICCI dataset are invited to visit the project's webpages (www.esa-seaice-cci.org).

1.4 Glossary

Acronym	Description
AMSR	Advanced Microwave Scanning Radiometer
ATBD	Algorithm Theoretical Basis Document
CCI	Climate Change Initiative
CDOP	Continuous Developments and Operations Phase
CDR	Climate Data Record
DMI	Danish Meteorological Institute
DMSP	Defence Meteorological Satellite Program
ECMWF	European Centre for Medium range Weather Forecast
ESA	European Space Agency
EUMETSAT	European Organization for the Exploitation of Meteorological Satellites
FCDR	Fundamental Climate Data Record
FoV	Field Of View
FYI	First Year Ice
GR	Gradient Ratio
MET	Norwegian Meteorological Institute

NASA	National Aeronautics and Space Administration
NH	Northern Hemisphere
NSIDC	National Snow and Ice Data Center
NWP	Numerical Weather Prediction
OSI SAF	Ocean and Sea Ice Satellite Application Facility
PCR	Product Consolidation Review
RTM	Radiative Transfer Model
SAR	Synthetic Aperture Radar
SH	Southern Hemisphere
SIC	Sea Ice Concentration
SICCI	ESA CCI Sea Ice project
SMMR	Scanning Multichannel Microwave Radiometer
SSM/I	Special Sensor Microwave/Imager
SSMIS	Special Sensor Microwave Imager Sounder
Tb	Brightness Temperature
TBC	To Be Confirmed
TBD	To Be Determined
TBW	To Be Written
WF	Weather Filter

1.5 Applicable documents

- OSI SAF CDOP-2 Product Requirement Document, v2.5.
- OSI SAF Global Sea Ice Concentration Reprocessing Product User Manual (OSI-409), Version 1.3. Available at http://osisaf.met.no/docs.
- OSI SAF Global Sea Ice Concentration Reprocessing Validation Report (OSI-409), Version 1.3. Available at http://osisaf.met.no/docs.

2 Input Data

This chapter describes the SMMR, SSM/I and SSMIS satellite data as well as numerical weather prediction (NWP) data used for atmospheric correction of the brightness temperature. The SMMR, SSM/I, and SSMIS data are all from the Fundamental Climate Data Record (FCDR) V2 (2015) from the EUMETSAT Climate Monitoring Satellite Application Facility (CM-SAF, http://dx.doi.org/10.5676/EUM_SAF_CM/FCDR_MWI/V002).

2.1 The SMMR data

The Scanning Multichannel Microwave Radiometer (SMMR) instrument on board the Nimbus 7 satellite operated from October 1978 to August 1987 (Gloersen et al., 1992). The instrument was operated only every second day, due to power supply limitations. The instrument had 10 channels, from the six Dicke radiometers, at five frequencies (6.6, 10.7, 18.0, 21.0, 37.0 GHz) and vertical and horizontal polarization. The scanning across track was ensured by tilting the reflector from side to side while maintaining constant incidence angle on the ground of about 50.2°. The scan track on the ground formed a 780 km wide arc in front of the satellite (Gloersen and Barath, 1977). Because of the satellite orbit inclination and swath width there is no coverage poleward of 84°. The SMMR instrument is further described in http://nsidc.org/data/docs/daac/smmr_instrument.gd.html and in the CM-SAF documentation.

Frequency (GHz)	**Polarizations**	**Sampling** (average)	**Field of view**	
			Along-track	**Cross-track**
6.6	H,V	25 km	148 km	95 km
10.7	H,V	25 km	91 km	59 km
18.0	H,V	25 km	55 km	41 km
21.0	H,V	25 km	46 km	30 km
37.0	H,V	25 km	27 km	18 km

Table 1: Characteristics of the Nimbus 7 SMMR channels (Gloersen and Barath, 1977).

2.2 The SSM/I data

The Special Sensor Microwave/Imager (SSM/I) sensors on board the Defence Meteorological Satellite Program (DMSP) started its record with the F08 satellite on 9th July 1987, shortly before the SMMR ceased to operate on 20th August 1987. The different SSM/I instrument records are summarised in Table 2. The SSM/I is a total power radiometer, with a conical scan measuring the upwelling radiation from the Earth at a constant incidence angle of about 53.1° at 7 different channels. The channels are summarised in Table 3. The swath width is about 1400km.

The Special Sensor Microwave/Imager (SSM/I) data set used for this reprocessing was prepared by EUMETSAT CM SAF and covers the period of available satellites with SSMI/I instruments from 1987 to 2008. The different satellites and covered

periods are listed in Table 2. Note that the dates in Table 2 are for the available SSM/I data in the CM-SAF FCDR. The lifetime of the instruments or platforms might be longer.

The SSM/I instrument has five low frequency channels similar to SMMR. In addition, two higher frequency channels, with twice the sampling rate, are available on the SSM/I. The characteristics of these channels are listed in Table 3. The 85 GHz channels had a malfunction on F08, so they are only useful starting with the F10 satellite. The 85 GHz are not used for OSI-450.

Satellite	Period covered
F08	Jul 1987 – Dec 1991
F10	Jan 1991 - Nov 1997
F11	Jan 1992 – Dec 1999
F13	May 1995 – Dec 2008
F14	May 1997 – Aug 2008
F15	Feb 2000 – Jul 2006

Table 2: The different satellite missions carrying the SSM/I instrument and the periods they cover.

Frequency (GHz)	Polarizations	Sampling	Footprint size	
			Along-track	Cross-track
19.35	H,V	25 km	69 km	43 km
22.235	V	25 km	50 km	40 km
37.0	H,V	25 km	37 km	28 km
85.5	H,V	12.5 km	15 km	13 km

Table 3: Characteristics of the different SSM/I channels (from Wentz, 1991).

Readers interested in the processing, calibration and quality check steps applied in the FCDR will find many more details in the CM-SAF documentation (Fennig et al 2015).

2.3 The SSMIS data

The SSMIS is a polar orbiting conically scanning radiometer with constant incidence angle around 53.1° and a swath width of about 1700 km. It has window channels near 19, 37, 91, and 150 GHz and sounding channels near 22, 50, 60, and 183 GHz. All channels are available in both H and V polarization. The OSI-450 is using brightness temperature swath data of the 19V, the 37V and the 37H channels. At these channels, the SSMIS frequencies, sampling, geometry, and field-of-view are identical as those of the SSM/I (see above). Data from three DMSP platforms are used in OSI-450: F16 (Nov 2005 - Dec 2013), F17 (Dec 2006 - Dec 2015), and F18 (Mar 2010 - Dec 2015).

2.4 The ERA-Interim data

The brightness temperatures (Tb) are corrected explicitly for atmospheric contribution to the radiation. The correction uses a Radiative Transfer Model function (RTM) and requires atmosphere re-analysis data. For OSI-450, we use the global 3-hourly fields from ECMWF's ERA-Interim (Dee et al., 2011), which are accessed from the MARS archive. Note that ERA 40 and ECMWF operational forecasts were instead used in the OSI-409 series.

The following prognostic variables are taken from the ERA-Interim files and collocated with satellite swath data: wind speed, 2m air temperature, and total column water vapour. The methodology for this correction as well as the RTM used are introduced in a later section.

3 Algorithms

This chapter describes all the algorithms and methods used in the three main steps of the daily sea ice concentration calculations; the Level 2, Level 3 and Level 4 calculations. These three setups are illustrated in Figure 2, and details are provided in the following sub sections.

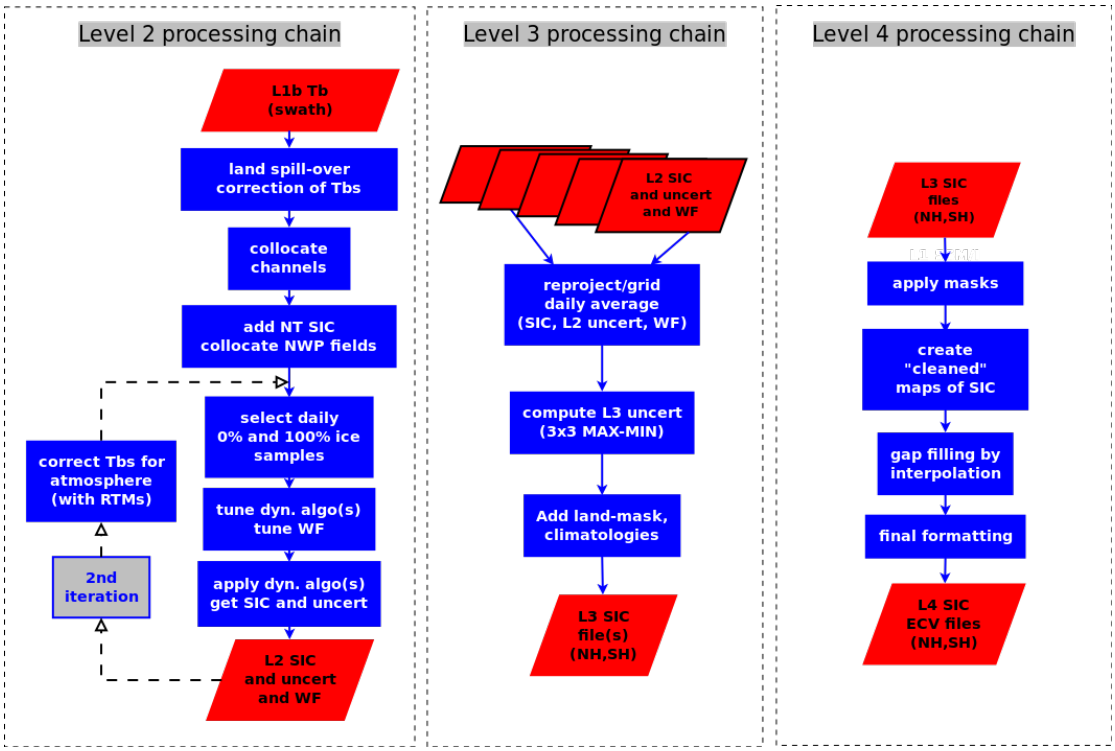

Figure 2: The three main steps in the daily sea ice concentration calculations.

3.1 Land spill-over correction of brightness temperatures

Due to the coarse resolution of the SMMR, SSM/I, and SSMIS radiometers (see Section 2), the brightness temperature (Tb) data are influenced by land up to 50 km from the coastline for the 19 GHz channels. The emissivity of land along the coastline is comparable to sea ice emissivity and much higher than water emissivity. This means that if there is open water or intermediate ice concentrations in the coastal zone, ice concentrations will be consistently overestimated. In the previous versions of the data set (OSI-409 series), a statistical method similar to Cavalieri et al. (1999) was implemented as a post-processing to the daily-gridded sea ice concentration maps. Such a method showed limitation and OSI-450 now introduces explicit land spill-over correction of the Tbs at all used channels on swath projection.

The correction algorithm is described in details in Maas and Kaleschke (2010). The basic principle is that, for each FoV in the swath file, one separates Tb into two

components, T_{sea} and $T_{land}\left(Tb=(1-\alpha)T_{sea}+\alpha T_{land}\right)$, where α is a convolution of the antenna gain function and land fraction of the footprint. Local T_{land} is calculated by using land fraction from high-resolution shoreline data in a defined neighbouring area. Then T_{sea} is computed from formula above.

The algorithm of Maass and Kaleschke (2010) was fully re-implemented in more efficient Python code, and the following modifications were tuned and implemented:

- Computation of the fraction of land α in each FoV is no longer computed on a projection plane, but in the view geometry of the instrument.
- The antenna pattern functions are approximated as Gaussian shapes indexed on the aperture angle from central view direction.
- The fraction of land α is computed from the same land mask as used otherwise in the SIC processing (e.g. for gridding and masking, see Section 3.4).

At the end of this step, Tbs of FoV that overlap coastal regions are corrected for the land emissivity, and can enter the sea ice concentration algorithms (see below).

3.2 Level-2 algorithms

The two ice concentration algorithms are the Bootstrap algorithm in frequency mode (Comiso, 1986; Comiso et al., 1997), and the Bristol algorithm (Smith, 1996). These two algorithms are used in combination as a hybrid algorithm.

3.2.1 The SICCI2 hybrid algorithms

The SICCI2 algorithm is a combination of two other algorithms, one dynamically optimized for providing Best accuracy at 0% ice concentration cases (BOW), and one dynamically optimized for providing best accuracy at 100% ice concentration cases (BICE). These optimized algorithm are described below. The combination works as follows:

$$c=c_0\times w_0+c_1\times w_{1,} \quad (1)$$

where c_o and w_0 are the output and weight for SIC from BOW dynamic algorithm, and c_1, w_1 are the output and weight for SIC from BICE dynamic algorithm.

```
if c0 < 0.7:
       w0 = 1.0
if (c0 >= 0.7 and c0 < 0.9):
       w0 = 1.0 - (c0-0.7)/(0.9-0.7)
if c0 >= 0.9:
       w0 = 0.0
w1 = 1.0 - w0
```

In the previous version of the OSISAF CDR (OSI-409 series) the algorithm was also a hybrid one, that used BOW = ComisoF (Comiso, 1986), and BICE = Bristol (Smith and Barrett, 1994, Smith, 1996). The weighting function was also slightly different, but was later found to give too much weight to Bristol results at low concentration values (Ivanova et al. 2015).

3.2.2 Dynamic SIC algorithms from triplet of Tbs

The concept of dynamic algorithm is first introduced in the ESA CCI Sea Ice (phase 2) project (SICCI2). In earlier efforts (OSI-409 series, SICCI1,…) the SIC algorithms (the way the brightness temperature channels are combined in algebraic equations, plus some coefficients of these questions, etc.) are “fixed”, but the tie-points of the algorithms are derived dynamically. The dynamic tie-points approach is adopted to consistently achieve 0 bias at low and high concentration values. The dynamic tie-points also allow accommodating to calibration differences between instruments, FCDRs, as well as sensor drift.

With the SICCI2 “dynamic algorithms”, the very equation of the algorithms are tuned to minimise the standard deviation of the retrieved SIC, while simultaneously achieving 0 bias. The dynamic algorithm thus has the capabilities of the dynamic tie-points, with the additional capability to reduce the retrieval noise.

The proposed new algorithm allows computing sea ice concentration as a linear combination of brightness temperatures Tb at three channels, e.g.:

$$ct = a \times Tb_{19V} + b \times Tb_{37V} + c \times Tb_{37H} + d \quad (2)$$

The 19 GHz and 37 GHz channels with vertical polarization and 37 GHz with horizontal polarization are acquired by the SMMR, SSM/I, and SSMIS instruments (see Section 2). These three channels – or their equivalent for Advanced Microwave Scanning Radiometer (AMSR-E and AMSR2) – have been used for many other published sea ice concentration algorithms.

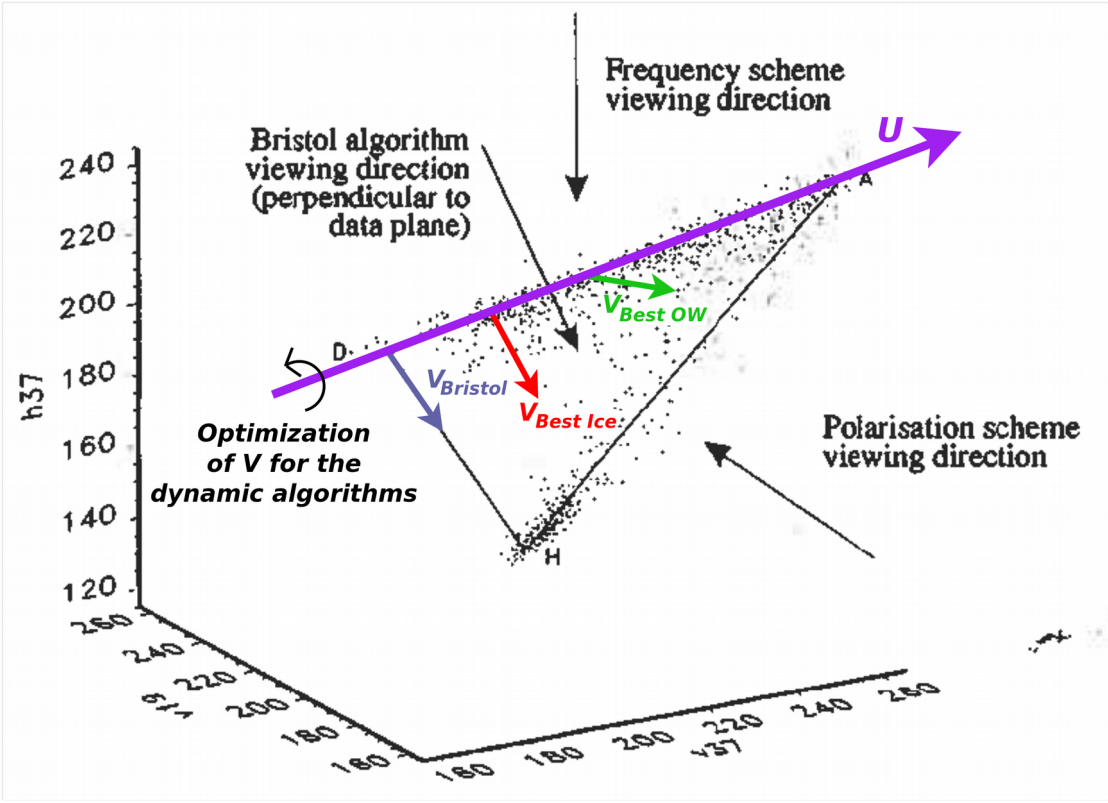

Figure 3: Three dimensional diagram of open water (H), and consolidated ice (ice line between D and A) brightness temperatures in a 19V, 37V, 37H space (black dots). The original figure is from Smith et al. (1996). The vectors u (violet), vBristol (blue), vBest-ice (red), and vBest-OW (green) are added, as well as an illustration of the optimization of the direction of V for the dynamic SICCI2LF algorithms. See text for more explanations.

Tuning of the dynamic algorithm involves finding an optimal plane in the three dimensional Tb space, on which any Tb triplet can be projected, and inside which the corresponding sea ice concentration can be computed. The algorithms are tuned against representative brightness temperature samples, one typical of 0% ice concentration cases (*ow*), and one typical of 100% ice concentration cases (*cice*). Each set holds hundreds or thousands of Tb triplets that are representative for these two extreme ice conditions. See Sections 3.2.4 for a description of how these samples are selected from satellite data.

The first step in the tuning of the algorithm is to perform a Principal Component Analysis (PCA) of the *cice* samples. In PCA, a matrix, $\boldsymbol{X}$, containing a set of possibly correlated variabilities, is transformed into a set of linearly uncorrelated variables (principle components). Here, $\boldsymbol{X}$ contains the brightness temperature measurements – in p columns (one for each channel) and n rows (with the individual brightness temperature measurements) – and with the mean of each column of $\boldsymbol{X}$ shifted to zero.

The PCA procedure gives the mean *cice* point, the three eigenvalues (sorted in decreasing order variance described) and the corresponding three eigenvectors. The magnitude of the eigenvalues describes the variance of the *cice* samples along

preferred directions (the eigenvectors) and around the mean *cice* point. At these channels, the largest variance is observed along the ice line, that extends between the typical signature (aka tie-point) of First Year Ice (FYI) and Multi Year Ice (MYI) in the Arctic (Type-A and Type-B in the Antarctic). The first eigenvector (noted *u*) returned by the PCA of the *cice* sample defines the ice line in the three dimensional Tb space, ta line that goes through the mean *cice* point. In typical, winter conditions, the first eigenvalue is an order of magnitude larger than the two others. These define two directions in the Tb space with less (2nd) and least (3rd) variance in the *cice* sample. The *ow* sample does not enter a PCA, but is simply averaged to find the mean *ow* point, that is the typical signature of open water conditions (aka the open water tie-point).

A sea ice concentration in the form of Eq. 1 can be described as a coordinate transform, that map a point in the three dimensional (3D) Tb space into the one-dimensional (1D) axis of sea ice concentration. Such a coordinate transform is the composition of 4 steps : 1) a projection of a 3D point onto a 2D plane, 2) in that plane, a projection of the 2D point onto a 1D axis, 3) a scaling of the 1D axis, and 4) a shift of its origin :

$$ct_v(Tb_{19V}, Tb_{37V}, Tb_{37H}) = \alpha(v_x Tb_{19V} + v_y Tb_{37V} + v_z Tb_{37H}) + \beta \quad (3)$$

By choosing v = (v_x, v_y, v_z) to be a unit vector perpendicular to *u* in the 3D Tb space (Figure 3), we ensure that all points along the cice line correspond to the same sea ice concentration value. The constant α is computed so that the difference between ct(*cice*) (the transformed mean *cice* point) and ct(*ow*) (the transformed mean *ow* point) is 1, and the constant β is such that ct(ow)=0.

Solving the optimization problem is to find two vectors v_{bice} (resp. v_{bow}) that are both perpendicular to *u* in the 3D space, and that lead to smallest standard deviation of ct(*cice*) (resp. ct(*ow*)). In practice, once *u* is computed from the Tb samples, a set of discretized rotation angles covering the range [-90:+90] is iterated upon. To each rotation angle, a new unit vector *v* is defined, that corresponds to a new algorithm (Figure 3). The algorithm is applied on both the *cice* and *ow* samples, and the standard deviation of ct(*cice*) and ct(*ow*) are recorded. While iterating, the vectors v_{bice} and v_{bow} are also kept. They correspond to a pair of algorithms ctBICE, and ctBOW that are optimized to the training *cice* and *ow* samples in terms of least standard deviation of retrieved ice concentration, and that have zero bias by construction. Thus, the coefficients to the algorithms are not only tuned dynamically to achieve zero biases, but also optimized to achieve least spread of retrieved ice concentrations.

The geometric descriptions above were all carried in a (19V, 37V, 37H) space, that feature two “higher frequency” channels with same wavelength but alternate polarization, and a “lower frequency” channel. The role of the “higher frequencies” is to control the spread of *cice* samples along a line, and offer a good base for PCA. They also bring finer spatial resolution to the retrieved sea ice concentration. The

addition of the “lower” frequency is to ensure sufficient dynamic range between *ow* and *cice* conditions, and thus aim at reducing retrieval noise. This is at the cost of bringing coarser spatial resolution into the algorithm.

The hybrid (Section 3.2.1) dynamic sea ice concentration algorithm using 19V, 37V, and 37H channels is named SICCI2LF (LF=Low Frequency) and is the algorithm used for OSI-450. The CDR produced in the SICCI2 projects, based on AMSR-E and AMSR2 instruments additionally introduces SICCI2VLF (VLF=Very Low Frequency, with 6V, 37V, and 37H) and SICCI2HF (HF=High Frequency, with 19V, 89V, and 89H). The SICCI2VLF and SICCI2HF are not featured in OSI-450 since the required channels are not consistently acquired through the SMMR, SSM/I and SSMIS time-series.

3.2.3 Atmospheric correction of Tb

As described in Andersen et al. (2006B) and confirmed in Ivanova et al. (2015), the accuracy of retrieved sea ice concentration can be greatly improved by using a Radiative Transfer Model (RTM) combined with surface and atmosphere fields from NWP re-analysis. This step is mostly similar to what was implemented in the OSI-409 series.

3.2.3.1 The radiative transfer model function for open water and sea ice

We use the RTM from Wentz (1983) for SMMR, and Wentz (1997) for SSM/I. The model function is using the simplified radiative transfer equation, which is adequate for many applications including this one, together with regressions describing the sensitivity to atmospheric and surface parameters. The radiative transfer equation for the top of the atmosphere brightness temperature, F, above a pure ocean surface is:

$$F_i(W,V,L) = TBU_i + \tau[E_i \times TS + (1-E_i)(\Omega_i \times TBD_i + \tau\, TBC)] \quad (4)$$

where V [mm] is the total water vapour, W [m/s] is the wind speed (at 10m) and L [mm] is the total liquid water in the atmospheric profile. *Ei* is the ocean surface emissivity, TBC [K] is the cosmic background radiation (2.7K), τ is the atmospheric transmittance, TBU [K] and TBD [K] are the up- and down-welling atmospheric brightness temperatures. TS [K] is the physical temperature (SST) and Ω is the reflection reduction factor due to wind induced surface roughness. The subscript *i* is for quantities that depend on the microwave channel (wavelength and polarization).

In the case of a mixed surface with two different emissivities (ocean and ice), this generalizes to:

$$\begin{aligned} F_i(W,V,L) = TBU_i + \tau_i * ((1-SIC) * E_{wi} * Tsea_i + SIC * Eice_i * Ti + \\ (1-SIC) * (1-Ewi) * (\Omega_i * TBD_i + \tau_i * TBC) + \\ SIC * (1-Eice_i) * (TBD_i + \tau_i * TBC)) \end{aligned} \quad (5)$$

where Tice is the ice effective temperature for each channel, and Tsea is the physical sea surface temperature. SIC is the sea ice concentration where 0 is open water and 1 is 100% ice.

3.2.3.2 Iterative double-difference scheme for atmospheric correction

As in the OSI-409 series, the atmospheric correction of brightness temperatures is achieved through a "double-difference" scheme similar to (but not identical to) that described in Andersen et al. (2006B).
The scheme evaluates $\delta \mathrm{Tbs}$ as the difference between two runs of the RTM.

$$Tb_{nwp} = F(W_{nwp}, V_{nwp}, L_{nwp} = 0; Ts, SIC_{ucorr}, \theta_o)$$
$$Tb_{ref} = F(0,0,0; Ts, SIC_{ucorr}, \theta_{instr})$$
$$\delta Tb = Tb_{nwp} - Tb_{ref}$$
$$Tb_{corr} = Tb_{instr} - \delta Tb$$

The RTM is described in the section above. θ_o is the incidence angle of the FoV, while θ_{instr} is the nominal incidence angle of the instrument series (see Section 2). The double-difference scheme used in OSI-450 is thus both a correction of the atmosphere influence on the Tbs (as predicted by the NWP fields) and a correction to a nominal incidence angle. The latter is especially effective at fixing the SSM/I F10 signal, that suffered from the platform's drift in orbit. Due to higher emissivity of sea ice than open water at the channels we use, the typical values δTb range from about 10 K over open water to few tenths of a Kelvin over consolidated sea ice. The Cloud Liquid Water (L) fields from global NWP fields (and ERA-Interim in particular) were found to not be accurate enough for being used in our atmospheric correction scheme. The Tbs are thus not corrected for L, and the induced remaining noise transfers into uncertainty in SIC.

Sea Ice Concentration is an input to the RTM calculation, and a first-guess value is thus required. It is taken as the SIC value computed by the SICCI2LF algorithm, using Tbs directly from the FCDR, not corrected for atmospheric effects (hence the notation SIC_{ucorr}). As in the OSI-409 series, RTM correction is implemented as an iteration, and the SIC algorithm is applied twice: once on uncorrected Tbs (Tb_{instr}), and once on corrected Tbs (Tb_{corr}). See also Figure 2.

3.2.4 Dynamical 0% and 100% SIC training samples

The dynamic algorithm SICCI2LF (Section 3.2.4) requires daily updated training samples of 0% (open water) and 100% (closed ice) conditions. The methodology for selecting these tie-points was updated since the OSI-409 series.

3.2.4.1 The closed-ice samples

It is assumed that ice concentrations larger than 95 % from the NASA Team (NT>95) algorithm (Cavalieri et al., 1984) are in fact a representation of 100 % ice on average. Additional tests ensure that samples are taken away from coastal regions, and inside a monthly climatology of ice extent. Figure 4 (left panels) shows an example of location of the closed ice samples. In an attempt to ensure temporal consistency between the SMMR and later instruments, the closed-ice samples for NH are only used for algorithm tuning if their latitude is less than 84N, which is the limit of the SMMR polar observation hole.

During winter, in the consolidated pack ice well within the ice edge, the ice concentration is very near 100 %. This has been established using high resolution SAR data, ship observations and by comparing the estimates from different ice concentration algorithms (Andersen et al., 2007). The apparent fluctuations in the derived ice concentration in the near 100% ice regime are primarily attributed to snow/ice surface emissivity variability around the tie-point signature and only secondarily to actual ice concentration fluctuations. Earlier investigations confirmed that NT was a robust estimation of high sea ice concentration, and one of the least correlated to those derived with the SICCI2LF algorithm.

Recent investigations during the SICCI2 projects additionally documented that NT is an acceptable choice for the purpose of selecting closed-ice samples in the summer melt season, albeit using winter tie-points (Kern et al. 2016).

3.2.4.2 The open water samples

The open water tie-point data are selected geographically along two belts on the northern and southern hemisphere. The belts extend outside a monthly maximum climatological ice extent, between 200 km and 350 km further away from the maximum extent. A land mask including the coastal zone ensures open water data only are kept. Samples south of 50N in the northern hemisphere are not used. Figure 4 (right panels) are an example of the location of the open water samples.

It is noteworthy that the OSI-409 series adopted a different approach to selection of OW training samples: they were selected in fixed areas in the Northern and Southern Atlantic Ocean, and were thus not as close to the ice edge as now implemented in OSI-450. This should lead to better accuracy of the retrieved SICs over open water in OSI-450 than in OSI-409 series.

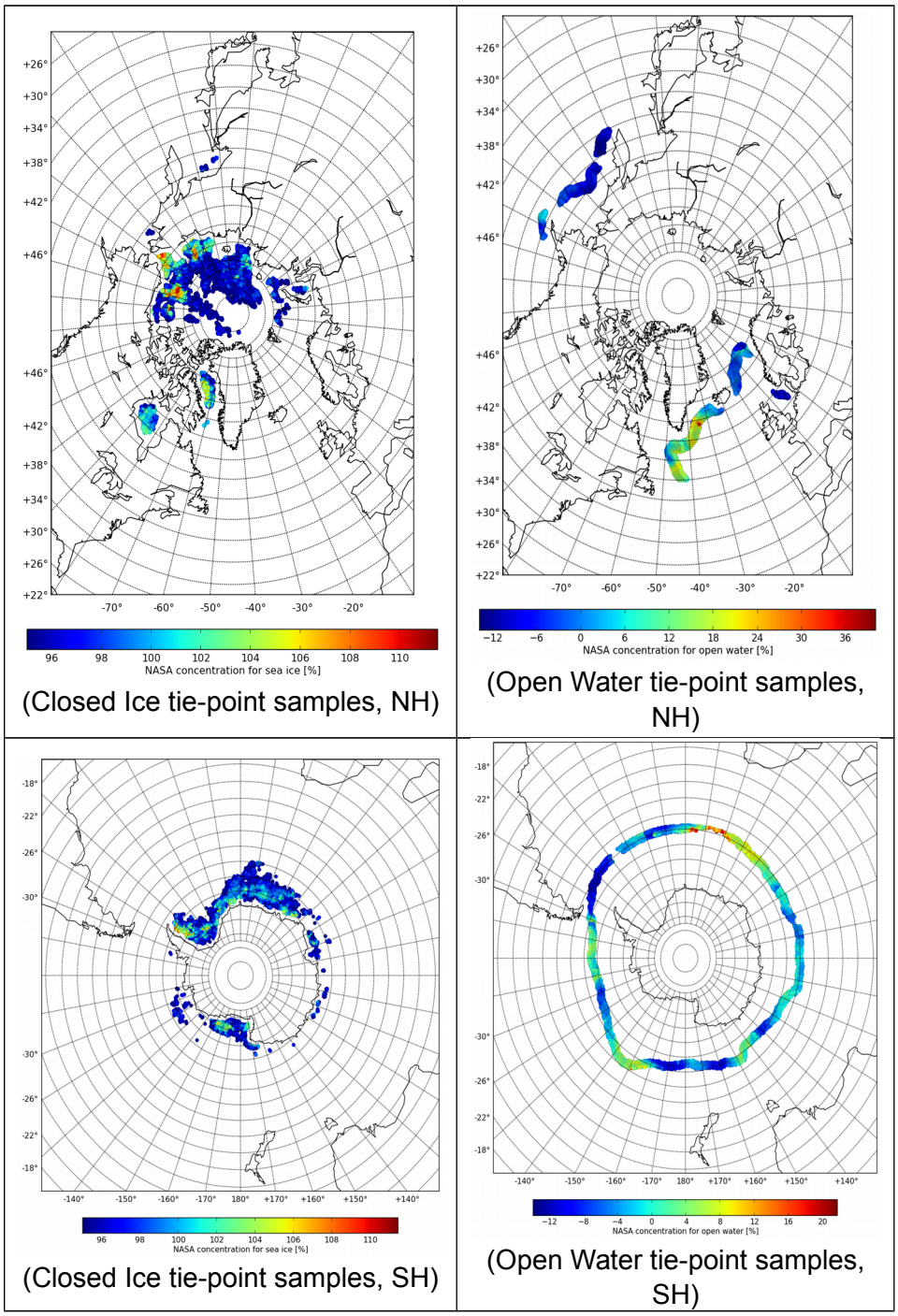

(Closed Ice tie-point samples, NH)

(Open Water tie-point samples, NH)

(Closed Ice tie-point samples, SH)

(Open Water tie-point samples, SH)

Figure 4: Example tie-point samples for Closed Ice (left) and Open Water (right), for NH (top) and SH (bottom). The colours scale with the NASA Team ice concentration, and is different for the Open Water and Closed Ice graphs.

3.2.4.3 Dynamic tuning: constantly updating the training samples

The OW and CICE data used for training the SICCI2LF algorithm are updated every day, and always contain [-7;+7 days] worth of daily samples. The daily samples are selected as described above. The time length of 15 days was chosen to be short enough to rapidly react to abrupt changes in emissivities over sea ice (e.g. at the onset of melting), yet long enough to not oscillate with the weather patterns over ocean (whose typical synoptic length scale is in the order of 5-7 days). The OSI-409 series used 31 days worth of daily samples.

The dynamic training of our algorithms is a key element of the OSISAF sea ice concentration algorithms since OSI-409 and is now also implemented in the operational near-real-time products (OSI-401 series). It allows to:

- Adapt to inter-season and inter-annual variations of the sea ice and open water emissivities;
- Cope with different calibration of different instruments in a series, or between different FCDRs;
- Cope with slightly different frequencies between different instruments (e.g. SMMR, SSM/I, and AMSR-E all have a different frequency around 19 and 37 GHz);
- Mitigate sensor drift (if not already mitigated by FCDR);

Compensate for trends potentially arising from use of NWP re-analysed data to correct the Tbs.

3.2.5 Weather Filter

Weather Filters (WFs) have been used in basically all SIC CDRs but the OSISAF ones. Weather filters combine instrument channels to detect when rather large SIC values are in fact noise due to atmospheric influence (mainly wind, water vapour, cloud effects), and should rather be reported as open water (0% ice concentration).

The original work by Gloersen and Cavalieri (1986) for SMMR was later updated by Cavalieri et al. (1992) for SSM/I, and has mostly been used as-is since then.

The Weather Filter by Cavalieri et al. (1992) detects as open water (and consequently forces SIC to 0%) all observations with either GR3719v > 0.050 and/or GR2219v > 0.045. The GR notation stands for Gradient Ratio and this quantity is computed as:

$$GR3719v = (Tb37v - Tb19v)/(Tb37v + Tb19v)$$
$$GR2219v = (Tb22v - Tb19v)/(Tb22v + Tb19v) \quad (6)$$

GR2219v is mostly meant for detecting water vapour effects, while GR3719v is effective at screening cloud contamination effects. However, both are designed to not discriminate between conditions with a calm ocean (little wind, little atmosphere wetness, etc.), conditions with heavy weather, and conditions with small concentration of sea ice (and/or thin sea ice). Tuning the two numerical thresholds

(0.050 and 0.045) to be less aggressive at removing true sea ice, automatically leads to allowing more atmospheric noise to be left unscreened. Using Weather Filters will consistently lead to removing an unknown amount of low concentration (and/or thin) sea ice, especially along the ice edge (Ivanova et al. 2015).

This is the very reason why the OSISAF (in its OSI-409 series) adopted explicit weather correction using NWP output and RTM (Andersen et al. 2006B) and not Weather Filters. This has resulted in SIC products that have not exactly 0% ice concentration in areas where one would not expect sea ice, and this noise has caused difficulties for some users.

The OSI-450 weather filter is introduced again in the algorithm baseline to provide additional, “pretty” SIC maps for applications that cannot handle the small scatter of SIC values in open water areas, and that are not too concerned about the loss of low concentration (and/or thin) sea ice.

The OSI-450 weather filter is computed from Tbs that have been corrected for atmospheric influence, and only features a test on GR3719v, not on GR2219v. There are two reasons for not using GR2219v: 1) a 22 GHz sounding channel is not available throughout the satellite time-series (SMMR’s is malfunctioning since start of mission and completely missing after 1985); and 2) the correction of water vapour using ERA-Interim data is effective enough and no additional screening is triggered by GR2219v.

The varying signature of sea ice and ocean emissivity with time and hemisphere, the different frequencies of the 19 and 37 GHz channels for different instruments, the varying effects of atmospheric correction all prevent the adoption of a fixed threshold (0.050) for screening with GR3719v. Instead, we adopt a dynamic approach to tune the threshold together with the SICCI2LF SIC algorithm, so that the WF will remove true ice only up to 10% SIC. Note that this corresponds to an average SIC threshold. Retrieval uncertainties are especially larger in the marginal ice zone and will result in different SIC values to be removed on a day-to-day basis.

The Weather Filter in OSI-450 is computed in swath projection, in the Level-2 chain, but only applied after gridding and daily averaging (see Section 3.3). The SIC values that enter the daily maps are thus directly from the SICCI2LF algorithms, and not screened by Weather Filter until at a later stage.

3.2.6 Level-2 uncertainties

Uncertainty estimates are needed when the ice concentration data are compared to other data sets or when the ice concentrations are assimilated into numerical models. The mean accuracy of some of the more common algorithms, used to compute ice concentration from SSM/I data, such as NASA Team and Bootstrap are reported to be 4-6 % in winter (Andersen et al., 2006A; Ivanova et al. 2015) but the actual value varies with instrument, region, ice condition, etc. and time-varying maps of uncertainties are needed. These are a key element of the OSISAF SIC CDRs, and

the approaches used in OSI-450 are rather similar to those used in the OSI-409 series.

We make the assumption the total uncertainty can be written as

$$\sigma_{tot}^2 = \sigma_{algo}^2 + \sigma_{smear}^2 \quad (7)$$

where σ_{algo} is the inherent uncertainty of the concentration algorithm, and σ_{smear} is the uncertainty, due to resampling to a grid where the sensor footprint covers more than one pixel. In this section, we only cover σ_{algo} while the approaches to σ_{smear} are documented in Section 3.3.2.

We first introduce how uncertainties are computed for a SIC algorithm, then how they must be combined for resulting in the uncertainty of an hybrid SIC algorithm like SICCI2LF (that combines a BestOW and a BestCICE algorithms, see section 3.2.1).

3.2.6.1 Algorithm and tie-point uncertainty

Both the water surface and ice surface emissivity variabilities result in ice concentration uncertainties. Emission and scattering in the atmosphere also affects the Tb's and the computed ice concentrations. Different algorithms have different sensitivities to these surface and atmospheric parameters (Andersen et al., 2006B; Ivanova et al., 2015).

Ice concentration can be interpreted as a superposition of water and ice:

$$\text{iceconc} = (1 - \alpha(\text{ic}))\,\text{water} + \alpha(\text{ic})\,\text{ice} \quad (8)$$

where α(ic) is the ice concentration calculated by the algorithm. The functional dependency between α(ic) and the calculated ice concentration *ic* is described by:

ic ≤ 0 , α = 0

0 < ic < 1, α = ic

ic ≥ 1 , α = 1

which can be written as

$$\alpha(ic) = \Pi_{0,1}(ic)\,ic + H(ic - 1) \quad (9)$$

where Πa,b (x) is the Boxcar function and H(x) the Heaviside step function. Using Equation 19 and assuming the uncertainty for the ice and water part are independent from each others, this leads to a total algorithmic uncertainty as

$$\sigma_{algo}(\alpha(ic)) = \sqrt{(1 - \alpha(ic))^2 \sigma^2{}_{water} + \alpha^2(ic)\sigma^2{}_{ice}} \quad (10)$$

where $\sigma_{water} = \sigma(IC(P_{openwater}))$ (*resp.* $\sigma_{ice} = \sigma(\text{IC}(P_{ice}))$) are the standard deviations of the SIC values retrieved by SICCI2LF for the open water (*resp.* closed ice) training samples. Since the training samples are updated everyday (Section

3.2.4) and depend on the hemisphere, the formula for computing the algorithm uncertainty is varying everyday, and on a hemispheric basis.

3.2.6.2 Uncertainty for the hybrid SICCI2LF algorithm.

The methodology above is applied to find both the Best OW and the Best ICE algorithm uncertainties at both ends of the concentration range (thus four σ values in total). The algorithm uncertainty of the SICCI2 algorithm (that combines BOW and BICE linearly, see section 3.2.1) is then computed as a linear combination of the variances. Using linear combination of variances as the resulting variance is in line with the hypothesis that the uncertainties of both BOW and BICE algorithms are strongly correlated to each others (ρ ~= +1). This approach does not allow for a reduction of uncertainties by combining two observations of SIC since they are not independent. Future studies might allow refining the approach, which is currently rather conservative.

The linear weighting is illustrated in the figure below:

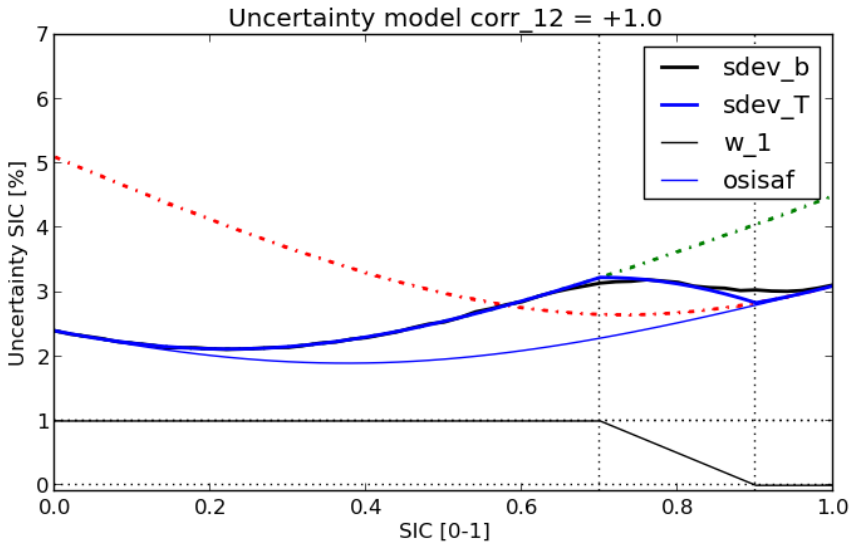

Figure 5: Illustration of the uncertainty merging of two algorithms (BOW in green, and BICE in red)

On Figure 5 above, the thin blue line is the uncertainty merging equation that was used in OSI-409 series, the thick blue line is the new merging equation, that takes into account the merging weights (black solid line at the bottom). The black thick line is the result of Monte Carlo simulations assessing that the new uncertainty merging model is more accurate than that from OSI-409.

3.3 Level 3 algorithms

The Level 3 step contains the gridding and averaging of the swath data to daily fields, calculation of smearing uncertainties, and preparation of masking fields.

3.3.1 Gridding and daily averaging

The gridding and daily averaging loads all satellite observation within 24 hours, centered on 12:00 UTC, and grid these to the final output grids. There are two such grids, one for the northern and one for the southern hemispheres. Both have a grid spacing of 25 km.

The gridding is based on a KD-Tree search based on the distance between the cartesian coordinates (Xg, Yg, Zg) of the centers of the target grid cells and the cartesian coordinates (Xs, Ys, Zs) of the center of the satellite's FoVs. The search for N neighbours is constrained to a radius of influence of 12.5 km around each grid cell. Once the N closest FoV neighbours are known for each grid cell, they are combined in a daily averaged value, all with equal weight. A large enough value is chosen for N that allows all available SSM/I and SSMIS swaths to be combined for each day.

The gridding is done for all areas with data coverage, including the coastal zone and land grid cells in the direct vicinity of ocean. A gridded field is made for all the variables that might be of interest: the SICCI2LF ice concentration estimates (both based on corrected and uncorrected Tbs), the algorithm uncertainties (combined as variances, not standard deviations), weather filters, etc.

3.3.2 Gridding and smearing uncertainty

The smearing uncertainty is the error due to the sensor footprint covering more than one pixel in the level 3 product grid. Foot-print sizes for the channels used for ice concentration mapping range from over 50 km, for the 19 GHz channels, to about 30 km, for the 37 GHz channels. Further, these foot-prints, of uneven size, are combined in the algorithms when computing the ice concentration and this leads to an additional smearing effect. We call this the foot-print mismatch error. The ice concentration data are represented on predefined and finer resolution grid (typically 10 or 25 km) The smearing and the foot-print mismatch error can not be estimated separately. However, the combined error can be simulated using high resolution ice concentration reference data and a model for the satellite measurement foot-print patterns.

The error is calculated taking cloud free 1 km MODIS images and assigning ice concentrations to all pixels based on the channel 1 brightness. For each pixel the corresponding brightness temperature is calculated for all relevant microwave channels based on standard tiepoints (Comiso et al. 1997). Using channel specific sensor footprints for weighting the ice concentration is calculated from the 1km brightness temperature image in the specified final resolution i.e. 10, 12, 25 and 50 km. This ice concentration is compared to the reference ice concentration (from MODIS), regridded to the same resolution. The standard deviation of the difference between these sets of ice concentration values is the standard deviation of the smeared points.

Using this approach, we parametrize the smearing uncertainty σ_{smear} with a proxy that measures the local variability of the ice concentraiton field. We found σ_{smear} to be proportional to the 3 x 3 pixel max - min sea ice concentration difference. This includes both the smearing and the foot-print mismatch and it is thereby the total smearing error. To avoid computing the smearing below the sea ice concentration

noise floor and not to exceed the range of values which were computed with the smearing simulator, the smearing error is:

```
if sigma_smear < sigma_SIC:
      sigma_smear = 0,
if sigma_smear >= sigma_SIC AND sigma_smear < 0.4:
      sigma_smear = 3 x 3 max - min sic difference,
if sigma_smear >= 0.4:
      sigma_smear = 0.4,
```

Where the sea ice concentration is a value between 0 and 1.

3.3.3 Climatological maximum extent masking

To mask out erroneous ice outside areas where sea ice is never likely to occur, a monthly maximum extent climatology is used. While the OSI-409 series used a climatology from NSIDC (http://nsidc.org/data/smmr_ssmi_ancillary/ocean_masks.html), that used for OSI-450 is updated, produced from the SIC maps of OSI-409. These maps are screened for gross errors, and processed so as to keep only sea ice where more than 25% of the years (1979-2015) had sufficient (SIC>40%) sea ice. An additional buffer zone is added outside this climatology: 150 km in both hemispheres.

The monthly climatology is used both for masking of the final product (see below) and for defining a monthly varying zone where to select the Open Water training samples (section 3.2.4).

3.3.4 Possible melting or high T2m flag

A quality flag using the ERA-Interim T2m (air temperature at 2 meters) field is added in the processing. The T2m ERA-Interim values that have been interpolated in time and space to each FoV are compared to +5C. The binary results of the flags (1 if T2m > 5C and 0 otherwise) are gridded and daily averaged with the same procedure as SIC (see above). The resulting map shows the frequency of “high T2m value” during the day, and can be used for triggering flags in the product files. Such a flag can however only be used for warning the users of possible melting events (or false sea ice), not correcting the SIC values. This is because of the uncertainty of ERA-Interim T2m at high latitudes, and the possible trends it could carry into the final SIC product.

3.4 Level 4 algorithms

This Level 4 step contains gap filling by interpolation of the areas with missing data, applying masks and coastal corrections, and final formatting of the final ice concentration product.

3.4.1 Gap filling by interpolation

For easing the use of the reprocessing data set, it was decided that some level of spatial interpolation should be performed for reducing the occurrence of gaps. Only missing data are interpolated. Interpolated data points are clearly marked in the

product file, so that users can choose to discard them and only ingest retrievals that rely on satellite signal.

Data gaps can occur in several forms, such as missing scan lines, missing orbits and the polar observation hole (NH only). While simple spatial interpolation might be efficient in filling small gaps (e.g. one or two missing scan lines), it blurs the sea ice concentration features. This effect becomes overwhelming when large areas are missing. To overcome this issue, yet implementing a general approach for all cases, the ice concentration estimates from the previous and next daily products are used in the interpolation as well. In the case of SSM/I, it means that interpolation on a given date *D* uses pixels from 3 data files: *D-1*, *D* and *D+1*. We use *D-2*, *D*, and *D+2* for SMMR.

Gap-filling by interpolation is implemented in two steps: first a temporal interpolation, then a spatial interpolation.

3.4.1.1 Temporal interpolation

All gaps (ocean grid cells with missing SIC data) at day *D* are identified. For these gaps, the average of the SIC from *D-1* and *D+1*:

$$SIC_{i,j,D} = 0.5 * (SIC_{i,j,D-1} + SIC_{i,j,D+1}) \quad (11)$$

In cases where only one of the *D-1* or *D+1* maps have data at i,j coordinate, $SIC_{i,j,D}$ is set to this value. Many gaps will be filled by the temporal insterpolation step, but some will remain, for example the polar observation hole in the NH.

3.4.1.2 Spatial interpolation

If there are still gaps in the SIC map at day *D* after the temporal interpolation step, these are filled by spatial interpolation using only the data from day *D*. This is implemented by a Gaussian weighting function of the distance. Our investigations concluded that R = $|lat_{i,j}|$ (the absolute value of the latitude in degrees at grid cell i,j) is an appropriate value for one standard deviation of the weighting function. This radius allows longer interpolation lengths at high latitudes (where the polar observation hole is), than at lower latitude (where the data gaps are smaller, and often filled by the temporal interpolation step). The weight is additionally localized into a [-3R;+3R] x [-3R;+3R] neighbourhood of grid cell (i,j).

3.4.2 Total uncertainty

The total uncertainty (variance) is computed at this stage, as the sum of the variances of the (gridded and daily averaged) algorithm uncertainty (section 3.2.6), and of the smearing uncertainty (section 3.3.2):

$$\sigma^2_{tot} = \sigma^2_{algo} + \sigma^2_{smear} \quad (12)$$

Since some users have requested that the different uncertainty terms are provided, the final OSI SAF sea ice concentration product files provides the three level of uncertainties:

- total uncertainty,
- the algorithmic uncertainty,
- the smear uncertainty.

4 Conclusions

This Algorithm Theoretical Basis Document (ATBD) presents the algorithm baseline for the upcoming version of the Global Sea Ice Concentration Climate Data Record (OSI-450). Several improvements are implemented since the OSI-409 baseline. Many of these enhancements are contributed by the ESA Climate Change Initiative Sea Ice project phases. This R&D input is particularly acknowledged. Production of the OSI-450 CDR will take place during fall 2016, for a release later in the year.

5 References

Andersen, S., L. Toudal Pedersen, G. Heygster, R. Tonboe, and L Kaleschke, Intercomparison of passive microwave sea ice concentration retrievals over the high concentration Arctic sea ice. *Journal of Geophysical Research* 112, C08004, doi10.1029/2006JC003543, 2007.

Andersen, S., R. T. Tonboe and L. Kaleschke. Satellite thermal microwave sea ice concentration algorithm comparison. *Arctic Sea Ice Thickness: Past, Present and Future*, edited by Wadhams and Amanatidis. Climate Change and Natural Hazards Series 10, EUR 22416, 2006A.

Andersen, S., R. Tonboe, S. Kern, and H. Schyberg. Improved retrieval of sea ice total concentration from spaceborne passive microwave observations using Numerical Weather Prediction model fields: An intercomparison of nine algorithms. *Remote Sensing of Environment, 104, 374-392*, 2006B.

Cavalieri, D. J., J. Crawford, M. Drinkwater, W. J. Emery, D. T. Eppler, L. D. Farmer, M. Goodberlet, R. Jentz, A. Milman, C. Morris, R. Onstott, A. Schweiger, R. Shuchman, K. Steffen, C. T. Swift, C. Wackerman, and R. L. Weaver. 1992. *NASA sea ice validation program for the DMSP SSM/I: final report.* NASA Technical Memorandum 104559. National Aeronautics and Space Administration, Washington, D.C. 126 pages.

Comiso J.C, D.J. Cavalieri, C.L. Parkinson, and P. Gloersen. Passive microwave algorithms for sea ice concentration: A comparison of two techniques. *Remote Sensing of Environment* 60, 357-384, 1997.

Comiso J.C. Characteristics of arctic winter sea ice from satellite multispectral microwave observations. *Journal of Geophysical Research* 91(C1), 975-994, 1986.

Dee, D. P., Uppala, S. M., Simmons, A. J., Berrisford, P., Poli, P., Kobayashi, S., Andrae, U., Balmaseda, M. A., Balsamo, G., Bauer, P., Bechtold, P., Beljaars, A. C. M., van de Berg, L., Bidlot, J., Bormann, N., Delsol, C., Dragani, R., Fuentes, M., Geer, A. J., Haimberger, L., Healy, S. B., Hersbach, H., Hólm, E. V., Isaksen, L., Kållberg, P., Köhler, M., Matricardi, M., McNally, A. P., Monge-Sanz, B. M., Morcrette, J.-J., Park, B.-K., Peubey, C., de Rosnay, P., Tavolato, C., Thépaut, J.-N. and Vitart, F. (2011), The ERA-Interim reanalysis: configuration and performance of the data assimilation system. Q.J.R. Meteorol. Soc., 137: 553–597. doi: 10.1002/qj.828

Fennig, Karsten; Andersson, Axel; Schröder, Marc. (2015): Fundamental Climate Data Record of SSM/I / SSMIS Brightness Temperatures. Satellite Application Facility on Climate Monitoring. DOI:10.5676/EUM_SAF_CM/FCDR_MWI/V002. http://dx.doi.org/10.5676/EUM_SAF_CM/FCDR_MWI/V002

Gloersen, P., and F. T. Barath. A scanning multichannel microwave radiometer for Nimbus-G and SeaSat-A. *IEEE Journal of Oceanic Engineering OE-2*(2), 172-178, 1977.

Gloersen, P., W. J. Campbell, D. J. Cavalieri, J. C. Comiso, C. L. Parkinson, H. J. Zwally. Arctic and Antarctic sea ice, 1978-1987: satellite passive-microwave observations and analysis. *NASA SP-511*, Washington D. C., 1992.

Gloersen, P., and D. J. Cavalieri (1986), Reduction of weather effects in the calculation of sea ice concentration from microwave radiances, J. Geophys. Res., 91(C3), 3913–3919, doi:10.1029/JC091iC03p03913

Ivanova, N., Pedersen, L. T., Tonboe, R. T., Kern, S., Heygster, G., Lavergne, T., Sørensen, A., Saldo, R., Dybkjær, G., Brucker, L., and Shokr, M.: Inter-comparison and evaluation of sea ice algorithms: towards further identification of challenges and optimal approach using passive microwave observations, The Cryosphere, 9, 1797-1817, doi:10.5194/tc-9-1797-2015, 2015.

Kern, S., Rösel, A., Pedersen, L. T., Ivanova, N., Saldo, R., and Tonboe, R. T.: The impact of melt ponds on summertime microwave brightness temperatures and sea ice concentrations, The Cryosphere Discuss., doi:10.5194/tc-2015-202, in review, 2016.

Kunkee, D. B., G. A. Poe, D. J. Boucher, S. D. Swadley, Y. Hong, J. E. Wessel, and E. A. Uliana, 2008. Design and evaluation of the first special sensor microwave imager/sounder, IEEE Trans. Geo. Rem. Sens. 46(4), 863-883.

Kålberg, P., A. Simmons, S. Uppala, and M. Fuentes. The ERA-40 archive. *ERA-40 Project Report Series*, ECMWF, Reading, 2004.

MAAß, N. and KALESCHKE, L. (2010), Improving passive microwave sea ice concentration algorithms for coastal areas: applications to the Baltic Sea. Tellus A, 62: 393–410. doi: 10.1111/j.1600-0870.2010.00452.x

Meier, W. Scanning Multichannel Microwave radiometer (SMMR) reprocessing for EUMETSAT. *OSI SAF Visiting Scientist Report*. 9 pages, 2008.

Smith, D. M. Extraction of winter total sea ice concentration in the Greenland and Barents Seas from SSM/I data. *International Journal of Remote Sensing 17*(13), 2625-2646, 1996.

Wentz, F. J. A model function for ocean microwave brightness temperatures. *Journal of Geophysical Research 88*(C3), 1892-1908, 1983.

Wentz, F. J. A well-calibrated ocean algorithm for SSM/I. *Journal of Geophysical Research* 102(C4), 8703-8718, 1997.